Experimental and computational studies of phase shift lithography with binary elastomeric masks

Joana Maria, Viktor Malyarchuk, Jeff White, and John A. Rogers[a)]
Department of Materials Science and Engineering, Department of Chemistry, Beckman Institute for Advanced Science and Technology, Frederick Seitz Materials Research Laboratory, University of Illinois at Urbana-Champaign, 1304 West Green Street, Urbana, Illinois 61801

(Received 28 September 2005; accepted 13 February 2006; published 24 March 2006)

This article presents experimental and computational studies of a phase shifting photolithographic technique that uses binary elastomeric phase masks in conformal contact with layers of photoresist. The work incorporates optimized masks formed by casting and curing prepolymers to the elastomer poly(dimethylsiloxane) against anisotropically etched structures of single crystal silicon on SiO_2/Si. Scanning optical microscopy and full-vector finite element computations reveal the important near field and proximity optical effects. Representative structures fabricated with this technique, including several that exploit subtle features in the intensity distributions, illustrate some of the capabilities. © *2006 American Vacuum Society.* [DOI: 10.1116/1.2184321]

I. INTRODUCTION

Advances in nanoscience and nanotechnology depend on nanofabrication techniques that can form optical, electronic, or biological structures, simply and inexpensively. In addition, as the requirements in resolution in microelectronics increase, so does the need for low cost and high throughput alternatives for projection mode lithography and electron beam lithography. As a result, there is a growing interest in photolithographic techniques that use optical near field or proximity effects for nanopatterning. Methods that exploit scanning subwavelength light sources[1–4] can achieve high resolution, but they are inherently slow unless they can be implemented with massively parallel arrays of light sources. Contact mode exposures through rigid chromeless phase shifting masks,[5,6] embedded-amplitude masks,[7–11] or elastomeric masks[12–17] provide powerful patterning capabilities that can be applied to large areas in a single step. A detailed understanding of the optics of these methods is critical to optimizing their performance and maximizing the range of structures that can be patterned with them. Such an understanding is also important to related optical techniques that can pattern three dimensional (3D) structures in transparent photosensitive polymers.[18,19] This article presents comprehensive experimental and computational studies of a class of technique that uses conformable, elastomeric phase masks. Scanning optical microscopy, photolithographic exposures, and full-vector finite element computations reveal the near field and proximity optics associated with masks that have well controlled geometries. Patterning capabilities that rely on subtle structures in the intensity distributions are presented. The results may be useful for a variety of applications that can benefit from the ability to perform low cost, two and three dimensional nanopatterning over large areas with simple experimental setups.

a)Electronic mail: jrogers@uiuc.edu

II. EXPERIMENT

A. Fabrication of phase masks with well controlled geometries

Figure 1 summarizes the steps for forming phase masks with well controlled geometries. The process uses a casting and curing procedure to produce elastomeric masks from structures of relief (i.e., "masters") defined by lithography and anisotropic etching. First, dry thermal oxidation (1100 °C, 30 min) of a silicon-on-insulator (SOI) wafer (University Wafer; ⟨110⟩ top silicon orientation with a thickness of 2.5 ± 0.5 μm, SiO_2 with a thickness of 1 μm, and ⟨100⟩ substrate silicon with a thickness of 500 μm) formed a SiO_2 layer with a thickness ~60 nm. Photolithography (Karl Suss Mask aligner; Model MJB3) defined lines of a thin layer of photoresist (Shipley 1805; spin cast at 3000 rpm for 30 s; thickness ~500 nm) oriented along the ⟨110⟩ direction. Reactive ion etching (RIE) (Plasma-Therm 790 Series) of the SiO_2 not protected by the photoresist with CF_4 for ~4.7 min (40 SCCM (SCCM denotes cubic centimeter per minute at STP) of CF_4, pressure=50 mTorr, power=100 W) created a SiO_2 etch mask for the underlying silicon. Removing the resist with an oxygen plasma (20 SCCM of O_2, pressure =50 mTorr, power=200 W, and time= ~5 min) and then etching the top silicon layer with 50% KOH solution at 90 °C removed the silicon in the regions not protected by the SiO_2. The ⟨110⟩ orientation of the top silicon leads to extremely smooth, vertical etched sidewalls. This procedure formed structures consisting of parallel lines and spaces (between 1 and 20 μm) that served as the masters for elastomeric phase masks. Other, nonoptimized, masters consisted of patterns of photoresist, defined by contact or projection mode photolithography, on silicon wafers. The profiles of relief in these cases were roughly vertical with reasonably smooth surfaces, although not as well controlled as those on the SOI wafers.

Exposing the masters to a vapor of a fluorinated silane formed a nonstick layer on the SiO_2 surfaces. Casting and

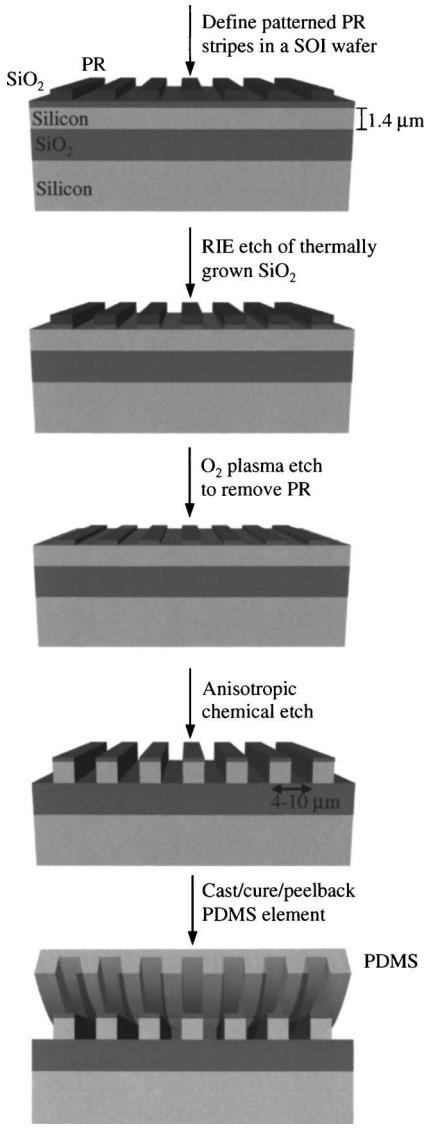

FIG. 1. Schematic illustration of the steps for fabricating PDMS phase masks with vertical sidewalls. Growth of a thin layer (~60 nm) of thermal SiO_2 on the SOI wafer followed by photolithography and RIE generates a SiO_2 etch mask for the silicon. Vertical sidewalls are produced by anisotropic chemical etching with KOH. Casting and curing PDMS on top of such a structure, after forming a fluorinated silane monolayer to prevent adhesion between the PDMS and SiO_2, generate the phase masks. Many masks can be generated from a single master.

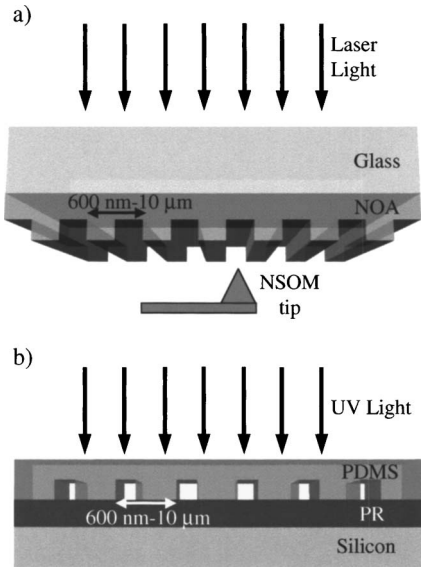

FIG. 2. Schematic illustrations for near field optical imaging and photolithographic use of PDMS phase masks. Part (a) shows the arrangement for near field scanning optical microscope (NSOM) measurements on a polyurethane replica of the PDMS phase mask. (PDMS is not used directly because its soft surface is difficult to measure using the AFM style tip of our microscope.) The NSOM tip is fixed in the plane of the mask; a stepper motor controls the distance between it and the mask. A piezoscanner translates the mask relative to the tip without changing the separation of its surface from the tip. Part (b) shows the method for using the mask to expose a thin uniform layer of photoresist on a substrate. The low modulus of the PDMS mask enables it to establish conformal contact with the resist, without applied pressure. After exposing the resist to ultraviolet light that passes through the transparent PDMS mask, the mask is removed and the photoresist is developed. The resulting structures are defined by the pattern of intensity at the surface of the mask.

thermally curing (65 °C, 2 h) a prepolymer to the elastomer polydimethylsiloxane (PDMS) (Sylgard 184, Dow Corning) against these masters,[14,15] and then peeling away the PDMS yielded the phase masks. Many such masks could be generated from a single master; each mask could be used many times without degradation.

Polyurethane (PU) replicas of these masks were used for the optical imaging measurements, because sticking of the tips of our scanning near field optical microscope (described below) to the PDMS made it difficult to measure the intensities at the surface of the PDMS masks. The replicas were made by bringing a mask into contact with three or four drops of polyurethane (Norland Optical Adhesive 73, Norland Products Inc.) on a glass slide, curing the PU by flood exposing it to UV light from a mercury lamp (350–380 nm, dose of 70 J/cm^2, and PU thickness ~1 mm) through the PDMS and then peeling away the mask.

B. Scanning optical microscopy

Measurements with a near field scanning optical microscope (NSOM) (Alpha SNOM from WITec Instruments Corp.) revealed the distributions of intensity formed by passage of laser light (HeCd at 442 nm) through PU replicas of line and space relief gratings with periods between 600 nm and 10 μm and depths between 330 nm and 1.42 μm, respectively [Fig. 2(a)]. We used specialized routines and setups with the NSOM to measure both the near fields at the surface of the mask as well as the propagating fields in proximity (i.e., within a few microns) to its surface. The central part of the NSOM is the scanning head, which consists of a tip holder and a scanning stage that serves as a mount for the samples. The tip and the focused output of the laser (focusing with a microscope objective lens, magnification of 6.3, numerical aperture of 0.20, and spot size on the sample ~60 μm) were fixed in the plane of the mask. A stepper motor attached to the sample mount controlled the separation between the tip and sample. A separate, piezoscanning stage moved the sample laterally relative to the laser and tip. This

stage, together with control electronics, has nanometer precision in lateral movement. The same unit provided tip-sample distance control by employing a feedback loop, which was activated in our measurements only when the tip was in contact with the sample. The images consist of data scans collected by holding the tip-sample distance fixed, scanning the lateral position of the sample, changing the tip-sample distance, and then repeating this process.

C. Near field phase shift lithography

The PDMS masks form conformal, atomic scale contacts with flat, solid layers of photoresist.[20] This contact is established spontaneously, without applied pressure, when the mask contacts the resist. Generalized adhesion forces[20,21] guide this process and provide a simple and convenient method to align the mask (in angle and position in the surface normal direction) and to establish perfect contact (i.e., no physical gap) with the resist. PDMS is transparent to UV light with wavelengths greater than $\sim$300 nm.[22] Passing light from a mercury lamp through the PDMS while it is in conformal contact with a layer of resist exposes the resist to the intensity distribution that forms at the mask surface [Fig. 2(b)]. The patterning process involved establishing contact between the mask and resist, shining UV light through the mask, removing the mask, and then developing the resist. We note that optical micrographs collected in reflection mode through the transparent stamps while in contact with the resist showed no evidence (e.g., variations in interference colors) of mechanical sagging of the recessed features of relief, for the range of geometries studied here.

D. Finite element modeling

Computations were performed using FEMLab (Comsol, Inc.), a commercial partial differential equation solver that uses the finite element method with adaptive meshing, error control, and a variety of numerical solvers. We used a stationary linear and direct solver using Gaussian elimination; in one dimension (1D) and two dimensions (2D) this type of solver is faster and requires less tuning than iterative solvers. The electromagnetics module/electromagnetic waves submodule/in-plane waves application mode of this package modeled plane waves propagating through binary phase masks with infinite spatial extent along the grating and perpendicular to it. The in-plane waves application mode modulates problems with no variation in the z direction and with the electromagnetic field propagating in the x-y plane, which also is the modeling plane.

Modeling was performed for cases with the mask in free space and in contact with a thin layer of photoresist on silicon for both the transverse magnetic (TM) (electric field perpendicular to the grating wave vector) and the (transverse electric (TE) (electric field parallel to the grating wave vector) modes, and full-vector solutions of Maxwell's equations were obtained. The wavelengths of light were 365 and 442 nm for simulations of the lithography and microscopy measurements, respectively. (The effects of the finite chromatic bandwidth of the mercury lamp, particularly when that spectrum is convolved with the spectral response of the resist, are relatively small for most cases examined here.) The low-reflecting boundary condition $\mathbf{e}_z \cdot \mathbf{n} \times \sqrt{\mu}\mathbf{H} + \sqrt{\varepsilon}E_z = 2\sqrt{\varepsilon}E_{0z}$ ($\mathbf{e}_z$ is the polarization vector, $\mathbf{n}$ is the unit vector perpendicular to the boundary, μ is the permeability of vacuum, $\mathbf{H}$ is the magnetic field, ε is the permittivity of vacuum, E_z is the incident field, and E_{0z} is the inwards propagating field through the boundary; the electric field propagates in the x-y plane which is also the modeling plane and the z direction is then perpendicular to this plane) was used to define the boundaries that do not represent physical borders (i.e., top and bottom surfaces of the modeled system). This boundary condition allows for only a small part of the wave to be reflected; most of the incident wave propagates through this boundary. The incident wave was defined coming from the top surface of the phase mask by setting $E_z = 1$. To capture the infinite extent along the grating of the binary phase mask, periodic boundary conditions were chosen for the lateral edges. A perfect magnetic conductor (PMC) boundary condition was chosen for the TM mode of light, which imposes the tangential component of the magnetic field to be zero at the lateral edges. For the TE mode, a perfect electric conductor (PEC) boundary condition was used, meaning that the tangential component of the electric field at the lateral edges is zero.

The mesh can be controlled by adjusting the global element size of the mesh or the element size on an edge, domain, etc. In all computations a minimum of ten mesh elements per wavelength were used. The values of the refractive index of the materials used here were taken from the literature [$n_{\mathrm{PDMS}} = 1.43$, $n_{\mathrm{NOA}} = 1.56$, $n_{\mathrm{silicon}} = 6.54 + 2.89i$, and $n_{\mathrm{photoresist}} = 1.7426$)].[23–26]

III. RESULTS AND DISCUSSIONS

A. Masters and PDMS phase masks

The SOI masters provided a precise and reproducible ability to achieve well defined, smooth vertical sidewalls and horizontal surfaces in PDMS masks. This level of control is critically important in establishing meaningful quantitative comparisons between experiment and computations. Figure 3 shows low- and high-resolution scanning electron microscopy (SEM) images of a master with linewidths and spacings of 11 and 8.8 μm, respectively. This figure also shows a PDMS phase mask made from this same master. The mask faithfully replicates the vertical sidewalls in the SOI master. The photoresist masters (not shown here) offer less control over the relief shapes, although the sidewall slopes were typically within $\sim 10^\circ$ of vertical.

B. Optical measurements and computations

Figure 4 shows optical measurements obtained from polyurethane replicas of PDMS phase masks with different periodicities (from 600 nm to 10 μm); a corresponding schematic of the phase mask is represented in the top part of each NSOM image. Finite element computations appear in the left insets. Figure 5 presents measured and simulated linecuts

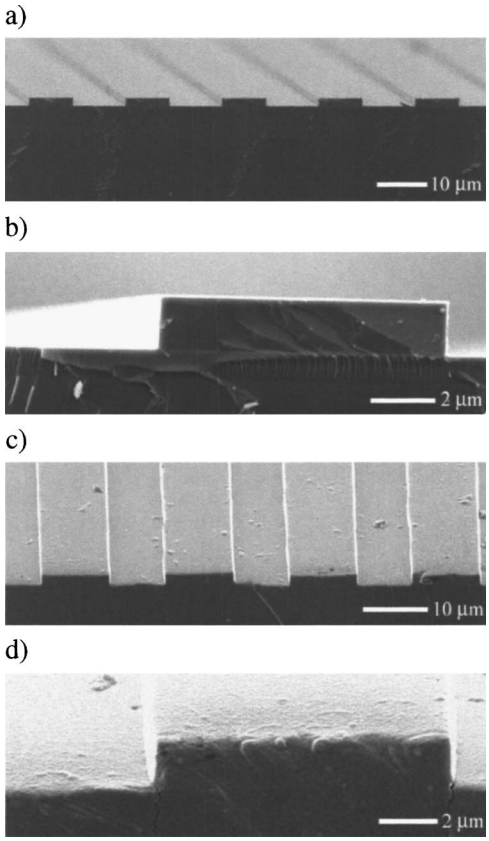

FIG. 3. Parts (a) and (b) show a low- and a high-resolution SEM image of a SOI master, respectively. Parts (c) and (d) show a low- and high-resolution SEM image of a PDMS phase mask with vertical sidewalls made from those masters. The grating phase mask has linewidths and spacings of 11 and 8.8 μm, respectively, and a relief depth of 1.62 μm.

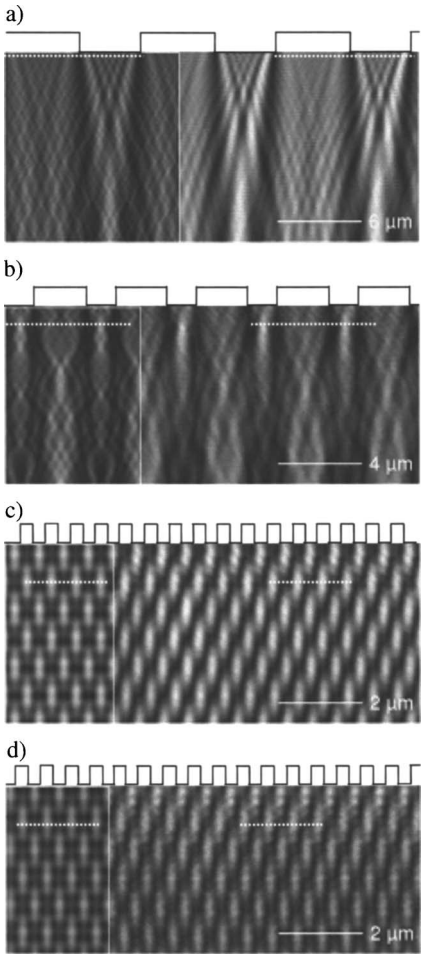

FIG. 4. Near field optical measurements and simulations (left insets) of light propagation through phase masks with different periodicities. The phase mask is represented on top of these linecuts for clarity. A HeCd laser produced the 442 nm light used for these measurements. Part (a) shows results for TM polarized light passing through a grating mask with linewidths and spacings of 4.4 and 5.6 μm, respectively. Part (b) shows results for TM polarized light passing through a grating mask with linewidths and spacings of 2.45 and 1.4 μm, respectively. Part (c) shows results for TM polarized light passing through a grating mask with linewidths and spacings of 300 nm each. Part (d) shows results for TE polarized light passing through a grating mask with linewidths and spacings of 300 nm each. The effects of polarization are significant only for small relief structures on the masks. In all cases, the computations accurately capture the features observed in the data.

corresponding to the depth locations illustrated by lines in Fig. 4. Parts (a) and (b) correspond to TM polarized light and phase masks with periodicities of 10 and 3.85 μm and relief depths of 1.42 and 1.25 μm, respectively. (The TE polarization differs only slightly from the TM case for both of these masks). Parts (c) and (d) show measurements for a phase mask with lines and spaces with 300 nm widths and relief depths of 330 nm with TM and TE polarizations, respectively. In all cases, the modeling agrees well with the experiment. Some previous work on lithography with these type of PDMS masks which have periodicities larger than the optical wavelength exploited the nulls in intensity that appear near the step edges of relief in the phase masks to pattern thin layers of photoresist.[14–17] The measurements and simulations shown in Figs. 4(a) and 4(b) for the NOA replicas illustrate that the widths of these features increase with the distance from the surface of the mask. The ability of the PDMS masks to form intimate contact with layers of resist therefore ensures maximum resolution when these nulls are used for photolithography. Other subtle features of this type of lithography process, such as the slight shift of the center positions of the nulls toward the recessed regions of the masks, were previously inferred from lithography experiments with PDMS masks but not well understood based on simple scalar theory;[15] they were suggested in some other more sophisticated computational work.[17,27] These effects are clearly observed in the optical measurements of the PU replicas and are quantitatively reproduced in the simulations of Fig. 4.

The contrast ratio associated with the deepest nulls is only a weak function of polarization for grating periods substantially larger than the optical wavelength, although the details of the features in the intensity distribution can depend on polarization. The polarization has an increasing importance as the period of the phase mask decreases; polarization dependent effects are pronounced for periods comparable to or less than the optical wavelength. The simulations and NSOM measurements of Figs. 4(c) and 4(d) for a 300 nm line and grating mask show that there is a difference in contrast for the two different modes of polarization of light, with the TM

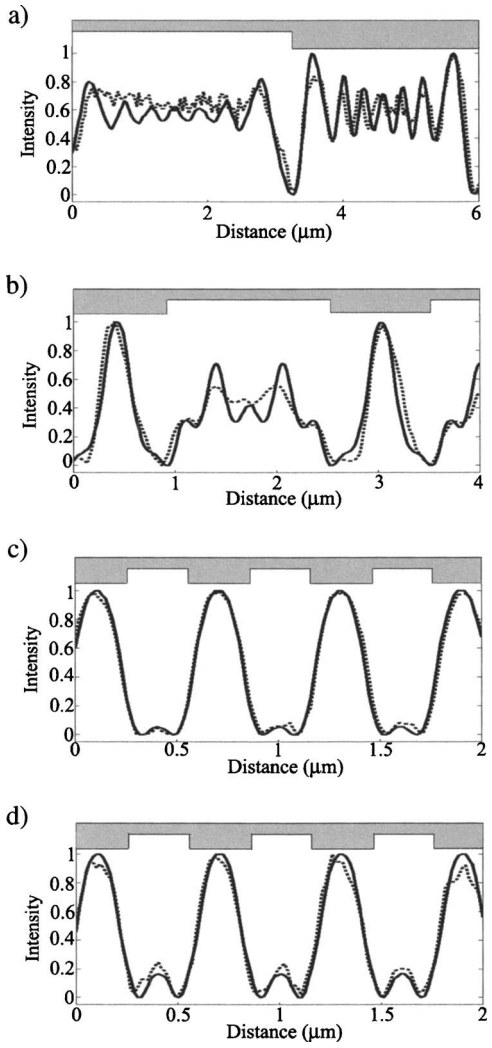

FIG. 5. Linecuts of the simulations (full line) and of the near field optical measurements (dashed line) from Fig. 4 made in the closest plane to the phase mask that exhibits maximum contrast in the intensity distribution. Parts (a)–(d) of this figure correspond to linecuts shown in Figs. 4(a)–4(d), respectively.

mode exhibiting a higher contrast. In this same short period regime, the intensity at the raised regions of relief is much larger than that at the recessed regions. This phenomenon can be considered as a subwavelength focusing effect where the raised and recessed relief features act effectively as convex and concave lenses, respectively. This effect can also be viewed as a result of the merging of adjacent nulls (center positions at the step edges but slightly shifted toward the recessed regions) and of adjacent peaks (center positions near the step edges, displaced toward the raised regions), as the period of the grating structure decreases. This same qualitative effect occurs in masks that have complex relief geometries (i.e., not just simple grating-type geometries) and can be exploited for patterning. Aspects of this phenomenon have been used by us and, in independent efforts, by a group at IBM.[12,13,15]

As Fig. 4 shows, for grating structures the bright and dark regions periodically vary from bright to dark, etc., with the distance from the surface of the mask. This recurrence with depth of particular patterns of intensity, which is pronounced for the case of the 600 nm period gratings but is also observable at longer distances in the larger period gratings, is due to the well known self-imaging, or Talbot effect for gratings.[28,29] For the 600 nm period mask, the Talbot self-imaging distances can be computed analytically using the equation $z=n^*Z_T=n^*(\lambda/\{1-[1-(\lambda/d)^2]^{1/2}\})=n^*1365.2$ nm since $d/\lambda<10$,[29] where d is the grating period, λ is the wavelength of the light (442 nm), and n is an integer. We measured a Talbot distance of $z=1360$ nm from the NSOM measurement and a distance of 1330 nm from the simulation, which are both close to the theoretical value. These types of two and three dimensional patterns of intensity can be exploited to form complex shapes using thick, transparent layers of resist.[18]

C. Near field phase shift lithography and computations

With low exposure doses and short development times, it is possible to produce relief structures in positive photoresist that reveal the intensity distributions near the surface of the PDMS, in a manner similar to that described previously for image reversal resists.[30] Comparing these structures to computations that include the PDMS mask in contact with resist on a silicon wafer provides a way to examine the validity of the computations for the actual lithographic process (in contrast to the transmission studies of Figs. 4 and 5). Figure 6 shows atomic force microscope (AFM) images, SEM images, and computations for the case of a PDMS mask with linewidths and spacings of 5.6 and 4.4 μm, respectively, and with a relief depth of 1.42 μm. This relief modulates the phase of the transmitted 365 nm light by $\sim 3.3\pi$. The mercury lamp in the mask aligner emits UV light at 365, 405, and 436 nm with relative intensities of 100%, 40%, and 50%, respectively. The lamp has other spectral lines at the wavelengths of 302, 313, and 334 nm but their relative intensities are below 35%. The 365 nm wavelength was used in the computational work for comparison with the experiment. The resist was $\sim$490 nm thick (Shipley 1805, spin coated at 3000 rpm for 30 s) and was exposed for 1.5 s (10 mW/cm^2) and developed for 15 s (Shipley developer 452). Figures 6(a) and 6(b) show SEM and AFM images of the patterned photoresist; Figs. 6(d) and 6(e) show computations.

The computed relief profiles were obtained by applying a cutoff filter to the intensity distribution evaluated at a depth of 50 nm into the photoresist. This cutoff filter simulates, in a simple way, the exposure and development processes: resist exposed at a level above or below the filter is removed or retained, respectively. This approach does not, of course, accurately account for all of the important aspects of the problem (e.g., the kinetics of dissolution of the resist, the nonlinearity of the exposure process, etc.), but at low exposure doses and short development times it does yield, with a suitable choice of cutoff intensity value, results that compare well with the experimental observations, including the subtle

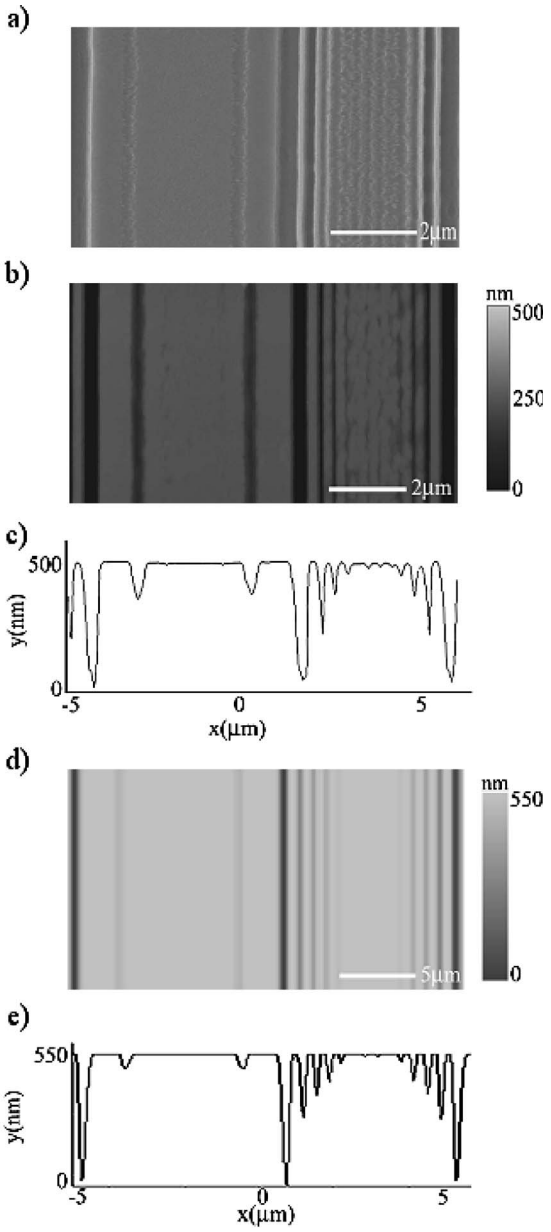

FIG. 6. Photoresist structure defined by near field phase shift lithography using a grating mask of linewidths and spacings of 5.6 and 4.4 μm, respectively, and a relief depth of 1.42 μm. Parts (a) and (b): SEM and AFM images of the photoresist (PR) structure, respectively. Part (c): experimental photoresist profile obtained from the AFM image on part (b) by generating an averaged linecut by averaging a set of individual linecuts collected along the patterned structure. Parts (d) and (e): computed photoresist profile and linecut for the TM mode of light passing through the grating phase mask described above.

fine structure, as illustrated in Fig. 6. This modeling, therefore, can provide a useful and predictive means to gain insight into the process. As an example, we note that the computations indicate that for this phase mask, the positive peaks of intensity are narrower (by a factor of ~0.4) than the "nulls" (as measured at 0.7 of the maximum; peak width ~225 nm a null width ~575 nm). This feature may provide a route to generating finer structures than have been possible in the past with this technique.

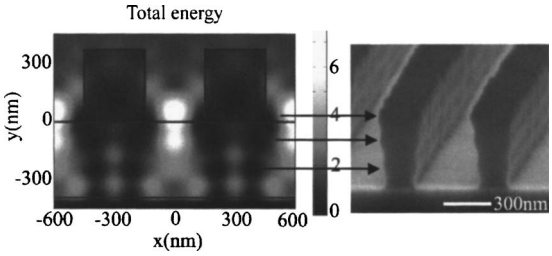

FIG. 7. Simulation (image on the left) and fully developed photoresist structure (image on the right) defined by near field phase shift lithography using a grating mask with 300 nm lines and spaces and a relief depth of 330 nm.

Figure 7 compares computations and experimental results for a fully developed photoresist structure formed by exposure through a PDMS mask with 300 nm lines and spaces and a relief depth of 330 nm. As in the previous case, the modeling results correspond well to the observed structures. The oscillations in the out-of-plane direction correspond to

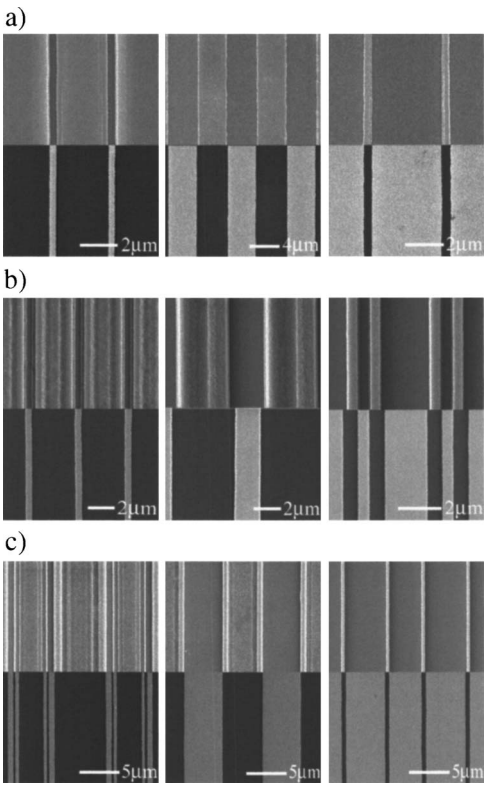

FIG. 8. Patterned metal structures (bottom of each image) formed by lift-off using patterns of photoresist (top of each image) defined by near field phase shift lithography. Three different phase masks, with different exposure and development conditions, were used to illustrate the variety of patterns that can be formed. The results of part (a) used a phase mask with 2 μm lines and spaces, and a relief depth of 420 nm. The exposure times (2.5, 4, and 5 s) increase from left to right; the development time (6 s) was the same in all cases. The results of part (b) used a phase mask with 1.4 μm lines and 2.45 μm spacings and a relief depth of 1.25 μm. The exposure times (1.5, 1.5, and 3 s) and development times (10, 20, and 10 s) varied from left to right, respectively. The results of part (c) used a phase mask with 5.6 μm lines and 4.4 μm spacings and a relief depth of 1.42 μm. The exposure times (1.5, 1.5, and 3 s) and development times (5, 20, and 5 s) varied from left to right, respectively.

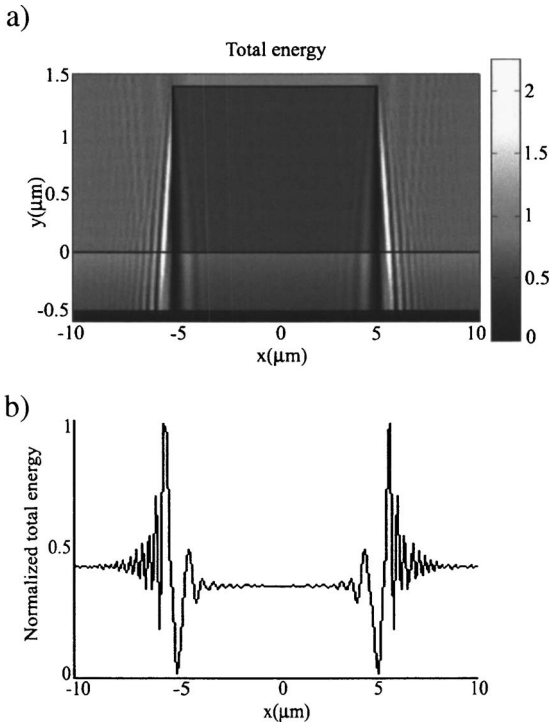

FIG. 9. Part (a) shows a simulation of TM polarized light propagating through a phase mask with linewidths and spacings of 10 μm and a relief depth of 1.4 μm in conformal contact with a 500 nm layer of photoresist on top of a silicon layer. Part (b) shows a linecut of the intensity of light made at a depth of 50 nm into the photoresist from the plot of part (a). Both images show a small difference in intensity between the contact and no contact regions of the phase mask.

standing waves generated from reflections at the interface between the resist and the underlying silicon wafer. This capability of directly printing subwavelength features that have the same geometry as the relief features on the mask provides a powerful tool for a range of applications in photonics and other areas.

In addition to the patterning of narrow lines of positive tone photoresist, as described in past work,[14,15,17] Fig. 8 shows a range of types of structures that can be produced, by exploiting other features of the distributions of intensity revealed by the computations. In the contact regions of the mask, there are positive peaks in the distribution of intensity adjacent to the nulls in intensity that occur at the phase mask edges. These peaks provide sufficient contrast to allow the development of trenches in the positive resist. The computed intensity distributions also show that this contrast increases with the relief depth of the phase mask; experimentally this effect was demonstrated by patterning different numbers of trenches by changing the mask relief depth. Figure 8(a) shows patterning of one trench in the resist using a phase mask with a relief height of 420 nm and periodicity of 4 μm (linewidth=2 μm), while Fig. 8(c) shows patterning of two trenches using a phase mask with a relief height of 1.42 μm and periodicity of 10 μm (linewidth 5.6 μm). Also illustrated in Fig. 8 is the capability of using the PDMS phase mask to form resist features in the overall geometry of the relief on the mask. The simulation results of Fig. 9 (TM polarized light propagating through a PDMS phase mask of linewidths and spacings of 10 μm and a relief depth of 1.4 μm in conformal contact with a thin layer of photoresist on top of a silicon substrate) provide some explanation for this experimentally observed patterning capability. This optical behavior, possibly amplified by the chemistry associated with exposure and development of the resist and other effects that were not directly modeled, allows the PDMS phase mask to be used effectively as a relatively weak amplitude mask that shadows the resist located under the recessed regions of relief.

IV. CONCLUSIONS

Near field optical microscopy measurements and full-vector finite element computations contribute to an improved understanding of the optics (near field and proximity) involved with phase shifting lithography using elastomeric and conformable phase masks. Representative structures that exploit this understanding demonstrate the range of patterning capabilities associated with these types of approaches.

ACKNOWLEDGMENTS

This work was supported by the US Department of Energy. SOI masters, photoresist patterns, and lift-off structures were fabricated in the Microfabrication and Crystal Growth Facility and NSOM measurements were performed at the Laser and Spectroscopy Facility of the Frederick Seitz Materials Research Laboratory, all of which is partially supported by the U.S. Department of Energy under Grant No. DEFG02-91-ER45439. This work was also funded by partial support from National Science Foundation under Grant No. DMI 03-55532. SEM, AFM imaging, and finite element modeling (FEM) simulations were performed in the installations of the Imaging Group of the Beckman Institute for Advanced Science and Technology. One of the authors (J.M.) gratefully acknowledges a fellowship from the Fundação para a Ciência e Tecnologia, MCES, Portugal.

[1] D. M. Eigler and E. K. Schweizer, Nature (London) **344**, 524 (1990).
[2] E. Betzig and J. K. Trautman, Science **257**, 189 (1992).
[3] S. Kraemer, R. R. Fuierer, and C. B. Gorman, Chem. Rev. (Washington, D.C.) **103**, 4367 (2003).
[4] D. Ginger, H. Zhang, and C. A. Mirkin, Angew. Chem., Int. Ed. **43**, 30 (2004).
[5] R. R. Kunz, M. Rothschild, and M. S. Yeung, J. Vac. Sci. Technol. B **21**, 78 (2003).
[6] H. Dang, J. L. P. Tan, and M. W. Horn, J. Vac. Sci. Technol. B **21**, 1143 (2003).
[7] J. G. Goodberlet, Appl. Phys. Lett. **76**, 667 (2000).
[8] J. G. Goodberlet and H. Kavak, Appl. Phys. Lett. **81**, 1315 (2002).
[9] M. M. Alkaisi, R. J. Blaikie, S. J. McNab, R. Cheung, and D. R. S. Cumming, Appl. Phys. Lett. **75**, 3560 (1999).
[10] M. M. Alkaisi, R. J. Blaikie, and S. J. McNab, Microelectron. Eng. **53**, 237 (2000).
[11] M. M. Alkaisi, R. J. Blaikie, and S. J. McNab, Adv. Mater. (Weinheim, Ger.) **13**, 877 (2001).
[12] H. Schmid, H. Biebuyck, B. Michel, and O. J. F. Martin, Appl. Phys. Lett. **72**, 2379 (1998).
[13] H. Schmid, H. Biebuyck, B. Michel, O. J. F. Martin, and N. B. Piller, J. Vac. Sci. Technol. B **16**, 3422 (1998).
[14] J. A. Rogers, K. E. Paul, R. J. Jackman, and G. M. Whitesides, Appl. Phys. Lett. **70**, 2658 (1997).

[15]J. A. Rogers, K. E. Paul, R. J. Jackman, and G. M. Whitesides, J. Vac. Sci. Technol. B **16**, 59 (1998).
[16]T. W. Odom, V. R. Thalladi, J. C. Love, and G. M. Whitesides, J. Am. Chem. Soc. **124**, 12112 (2002).
[17]J. Maria, S. Jeon, and J. A. Rogers, J. Photochem. Photobiol., A **166**, 149 (2004).
[18]S. Jeon, J.-U. Park, R. Cirelli, S. Yang, C. E. Heitzman, P. V. Braun, and P. J. A. Kenis, Proc. Natl. Acad. Sci. U.S.A. **101**, 12428 (2004).
[19]M. Campbell, D. N. Sharp, M. T. Harrison, R. G. Denning, and A. J. Turberfield, Nature (London) **404**, 53 (2000).
[20]K. J. Hsia, Y. Huang, E. Menard, J.-U. Park, W. Zhou, J. A. Rogers, and J. M. Fulton, Appl. Phys. Lett. **86**, 154106 (2005).
[21]K. G. Sharp, G. S. Blackman, N. J. Glassmaker, A. Jagota, and C. Y. Hui, Langmuir **20**, 6430 (2004).
[22]N. Chronis, G. L. Liu, K.-H. Jeong, and L. P. Lee, Opt. Express **11**, 2370 (2003).
[23]Product information supplied by Dow Corning at http://www.dowcorning.com/DataFiles/090007b5802e2039.pdf
[24]Product information supplied by Norland Products Inc. at https://www.norlandprod.com/adhesives/noa%2073.html
[25]E. Palik, *Handbook of Optical Constants of Solids* (Academic, New York, 1997).
[26]"Microposit S1800 Series Photo Resists" information supplied by Shipley at http://cmi.epfl.ch/materials/Data_S1800.pdf
[27]Z. Y. Li, Y. Yin, and Y. Xia, Appl. Phys. Lett. **78**, 2432 (2001).
[28]P. Latimer and R. F. Crouse, Appl. Opt. **31**, 80 (1992).
[29]E. Noponen and J. Turunen, Opt. Commun. **98**, 132 (1993).
[30]J. Aizenberg, J. A. Rogers, K. E. Paul, and G. M. Whitesides, Appl. Phys. Lett. **71**, 3773 (1997).